XVI. GASEOUS ELECTRONICS*

Academic and Research Staff

Prof. S. C. Brown	Prof. G. Bekefi	J. J. McCarthy
Prof. W. P. Allis	Prof. J. C. Ingraham	W. J. Mulligan
	Dr. D. R. Whitehouse	

Graduate Students

J. C. de Almeida Azevedo	G. A. Garosi	T. T. Wilheit, Jr.
A. J. Cohen	L. D. Pleasance	B. L. Wright
	J. A. Waletzko	

RESEARCH OBJECTIVES

A great deal of effort continues to be spent on the fundamental interaction of the particles of plasma physics. In this group we have concentrated on measuring diffusion coefficients, collision probabilities, particularly in partially ionized and fully ionized gases, and on the mechanism of production of radiation. Within the last few years we have studied the production of microwave radiation, and we are pushing this toward shorter and shorter wavelengths in the direction of the very long infrared. Our objective in this area is to study as many of the mechanisms involved in electron-atom and electron-molecule collisions as are susceptible to our microwave, infrared, and probe techniques.

S. C. Brown

A. MICROWAVE MEASUREMENTS OF A TIME-DEPENDENT ELECTRON VELOCITY DISTRIBUTION FUNCTION

The aim of the present work is to extract information about the velocity distribution of electrons in a plasma from measurements of the spectrum of emitted radiation. Microwave emission from plasmas has been a subject of continuing interest in this laboratory and the work reported here represents an extension of techniques developed by H. Fields, G. Bekefi, and S. C. Brown[1] for the study of cyclotron radiation from weakly ionized discharges. Basically, the method involves measurement of the power per unit frequency (intensity), $I_T(\omega)$, of radiation received from a plasma column inserted in a waveguide. For an optically thick plasma in thermal equilibrium, this intensity is given by $I_T(\omega) = kT$ in the limit $\hbar\omega \ll kT$. In this context, we define an effective radiation temperature, $T_r(\omega)$, by the relation $I_T(\omega) = kT_r(\omega)$. Thus, if the emission can be attributed to the motions of individual electrons (the weakly ionized case), the departure of $T_r(\omega)$ from a constant value reflects the departure of the electron velocity distribution, f(v), from a Maxwellian. These effects are most easily observed in the neighborhood of the electron cyclotron frequency of an applied magnetic field. In the present study, $T_r(\omega)$ and hence f(v) are examined as functions of time by sampling the radiation during

*This work is supported by the Joint Services Electronics Programs (U. S. Army, U. S. Navy, and U. S. Air Force) under Contract DA 36-039-AMC-03200(E).

various 1-μsec intervals in the afterglow of an argon discharge pulsed at a rate of 200 sec^{-1}.

Off resonance, the plasma column may not be fully opaque with respect to the radiation. To overcome this defect, it has been customary to provide an incident noise signal, I_o, at one end of the waveguide and to balance this against the emergent signal, I_1, received at the other. Thus, for a plasma slab of width X and absorption coefficient, $\alpha(x)$, the balance condition gives $I_o = I_1 = \epsilon I_o + (1-\epsilon)I_T$, where $\epsilon = \exp\left[-\int_o^X \alpha\, dx\right]$.

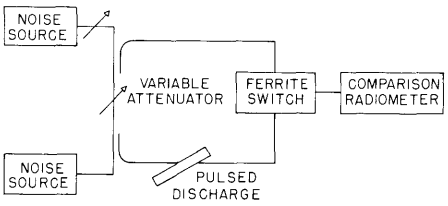

Fig. XVI-1.
Diagram of waveguide system.

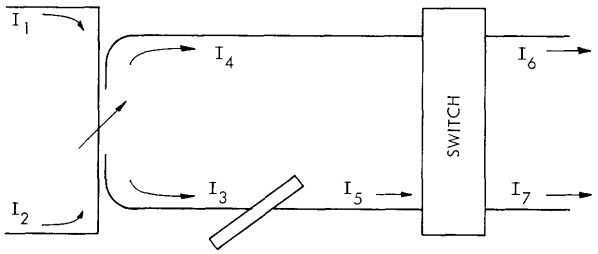

Fig. XVI-2.
Illustrating power flow.

The apparatus previously employed for this measurement was one in which I_o and I_1 were alternately sampled by a ferrite switching device before amplification and comparison in a synchronous detector. Because the isolation of the two channels in the switch could be made scarcely better than 20 db, serious errors arose from interference effects. Indeed, if ϵ were not small, that portion of I_1 coherent with I_o could, by leaking through the switch and interfering with the I_o sample, produce errors as great as 20% in the measurement of $T_r(\omega)$.

The present form of the waveguide system shown in Fig. XVI-1 is one which eliminates these effects. Directional couplers are used to feed the signals of two noise sources through the same variable attenuator and into the two branches of the system. Figure XVI-2 illustrates the power flow and the pertinent intensities in each section. Ferrite isolators are used to quench any reflected signals. The intensities I_3 and I_4 are related to the incident signals and the attenuator setting by

$$I_3 = \gamma\delta_1(I_1+\sigma_2 I_2) \qquad I_4 = \gamma\delta_2(I_2+\sigma_1 I_1),$$

where γ is the fraction of incident power transmitted through the variable attenuator, and the δ represent the 3-db losses in the couplers plus any fixed attenuations. The parameters σ_1 and σ_2 defined by these equations represent leakage across the coupler system and are not independent of γ. By choosing the sampled microwave frequency (3020 Mc) carefully, it was possible to obtain $\sigma < 10^{-3}$ over the range of γ used. The intensity I_5 is given as indicated above by $I_5 = \epsilon I_3 + (1-\epsilon)I_T$. Finally, I_6 and I_7 are

the received intensities when the switch samples the upper and lower branches. If we let β represent the leakage fraction between the two channels in the switch, these intensities are given by

$$I_6 = I_4 \oplus \beta_1 I_5 \qquad I_7 = I_5 \oplus \beta_2 I_6,$$

where $\oplus$ indicates that coherent components (originating from the same noise source) in the combined intensities must be added vectorially, not algebaically.

In practice, one adjusts I_1 with no plasma ($\epsilon=1$) to obtain the balance $I_6 = I_7$. Then, with the discharge on ($\epsilon \neq 1$), γ is varied to again balance the outputs. Working out the details, one finds the balance condition to be

$$\frac{I_T}{\gamma} = \frac{\delta_2}{\delta_1} I_2 \left[1 + \beta_1 - \beta_2 + \text{ terms of order } \frac{\sigma}{1-\epsilon} \text{ and } \frac{\sqrt{\beta\sigma}}{1-\epsilon} \right].$$

Thus I_T is proportional to γ, providing the terms that depend on σ and ϵ are small. The denominator $(1-\epsilon)$ merely reflects the loss of sensitivity off-resonance as the plasma becomes transparent. Indeed, for the effects of interference to be important, we only require σ, $\sqrt{\beta\sigma} < \frac{\Delta T}{T_r}$, where ΔT is the minimum detectable temperature of the radiometer. With $\Delta T \sim 10^{-2} T_r$, $\sigma < 10^{-3}$, and $\beta < 10^{-2}$, this inequality is satisfied. The constant relating T_r to γ is determined from a standard discharge of known temperature situated in the lower branch of the system.

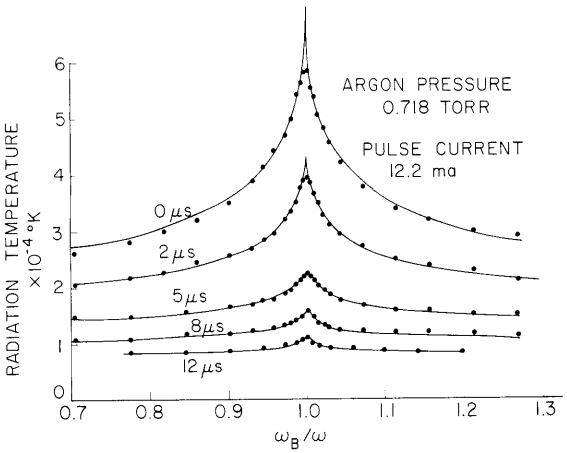

Fig. XVI-3.
Data sample.

A sample of data taken by this method is shown in Fig. XVI-3. Here, as is often the case, it is the magnetic field (ω_B), and not the sampled frequency ω, which is varied. The five curves give averages of $T_r(\omega/\omega_B)$ over 1-μsec intervals triggered at the afterglow times indicated. They represent the development of an originally non-Maxwellian distribution of electron velocities which is allowed to relax after the maintaining electric field is removed. The disappearance of the resonant peaks with time indicates the relaxation to a Maxwellian ($T_r(\omega)$ = constant). This is accompanied by a decrease in the mean electron energy.

To proceed beyond these general remarks, the detailed mechanisms of emission and absorption in the discharge must be considered. For the weakly ionized case, $T_r(\omega)$ has been shown[1] to depend on f(v) through the relation

$$kT_r(\omega) = -\frac{\int_0^\infty \frac{\nu(v)\, v^4}{\nu^2(v) + (\omega-\omega_B)^2} f(v)\, dv}{\int_0^\infty \frac{\nu(v)^4}{\nu^2(v) + (\omega-\omega_B)^2} \frac{\partial f}{\partial U}\, dv}$$

where $\nu(v)$ is the collision frequency for momentum transfer between electrons and neutral atoms, and $U = \frac{1}{2}mv^2$ is the electron energy. Here the electron velocity distribution, $f(v)$, is assumed to be isotropic – a condition well met by the experiment. If the denominator on the right side of this expression is moved over to the left, the result is a linear, homogeneous relation that, in principle, can be solved for $f(v)$ once $T_r(\omega/\omega_B)$ and $\nu(v)$ are known. The scatter in the measured values of T_r, however, will not permit determination of the details of $f(v)$. One must assume a form for $f(v)$ based on a few variable parameters which can then be adjusted to best fit the data. The form now employed is

$$f(v) = \frac{1}{\pi^{3/2} w_o^3} e^{-(v/w_o)^2} \sum_{n=0}^{N} F_n H_{2n}(v/w_o),$$

a Maxwellian term times a correction factor represented here as a finite sum of Hermite polynomials of even degree with variable coefficients F_n. If a value of the scale factor w_o is assumed, substitution of this form in the preceding relation yields, for each data point, a linear equation in the F_n. The equations thus generated are solved in the least-squares sense to obtain the best fit to $T_r(\omega)$ from the assumed form of $f(v)$. It should be noted that w_o may be chosen at will, but this freedom can be removed by requiring that the Maxwellian term have the same mean energy as $f(v)$. Furthermore, should $f(v)$ as given be negative beyond some cutoff velocity v_c, it is to be taken as strictly zero for $v > v_c$, and this fact must be incorporated in the evaluation of all required integrals.

A computer program has been developed to invert the relation between $T_r(\omega)$ and $f(v)$ in the manner described above. Tests show that if only a few independent coefficients are required, the results are fairly insensitive to errors of the kind that may be expected from the experiment. Figure XVI-4 shows the results of applying this treatment to the data of Fig. XVI-3. Plots of $v^2 f(v)$ are shown scaled for comparison in each case with a Maxwellian of the same mean energy, U. The first two curves are based on four independent coefficients; the rest, on three. The solid curves of Fig. XVI-3 give the fitted emission peaks based on these distributions. Roughly speaking, the time scale of relaxation is ~6 μsec – a figure not inconsistent with the rate expected from electron-electron collisions. Also apparent is a rapid initial decrease in U at a rate comparable

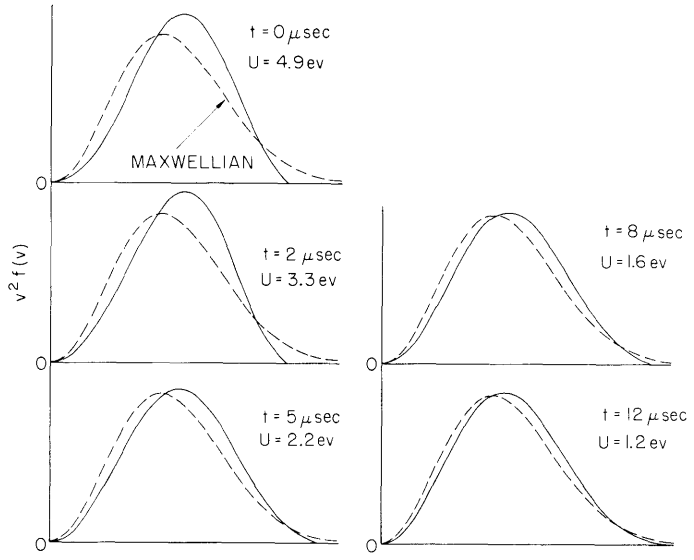

Fig. XVI-4. Results of computer program applied to data of Fig. XVI-3.

to that of the relaxation and far greater than expected from electron-atom collisions. The electron density in this case, as determined with a microwave cavity, remained constant at $\sim 1.0 \times 10^{10}$ cm^{-3} throughout the interval of interest.

Thus far, trials have been made with argon pressures of 0.2-0.8 torr and discharge currents of 10-35 ma. Further work will be devoted to extending these ranges and studying the effects of metastable atoms on the relaxation process.

B. L. Wright

References

1. H. Fields, G. Bekefi, and S. C. Brown, Phys. Rev. 129, 506 (1963).

B. RADIOFREQUENCY DIPOLE RESONANCE PROBE

In Quarterly Progress Report No. 74 (pages 91-98) D. F. Smith and G. Bekefi presented a theory for the spherical dipole resonance probe. They derived an expression for the complex admittance of a probe-plasma system in which the sheath region around the conducting dipole sphere was assumed to be a vacuum and the surrounding plasma extended to infinity. Numerical evaluations of the series solution show that the series converges very slowly. A large number of terms are required, because of the fringing electric fields in the region near the infinitesimal gap separating the two hemispheres of the idealized dipole. In order to minimize the effect of this small region of

the probe on the solution for the admittance, the probe hemispheres were constructed as shown in Fig. XVI-5. By rounding the edges of the hemisphere with a known curvature, it is possible to use the geometry of the experimental probe in the boundary

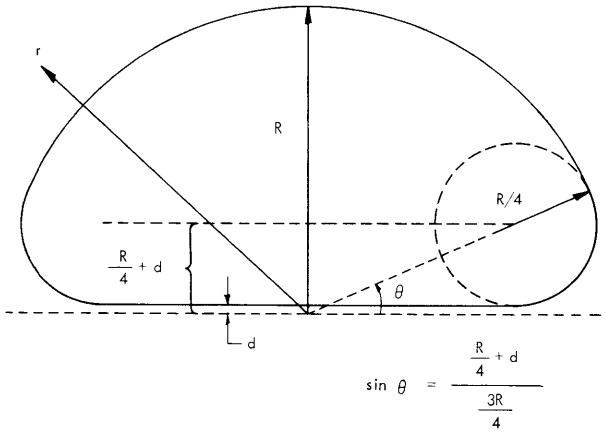

Fig. XVI-5. Dipole hemisphere.

conditions for the potential in the theoretical problem.

The potential on the surface of the probe is represented as a series of Legendre polynomials whose coefficients are determined by a least-squares fitting method. Under

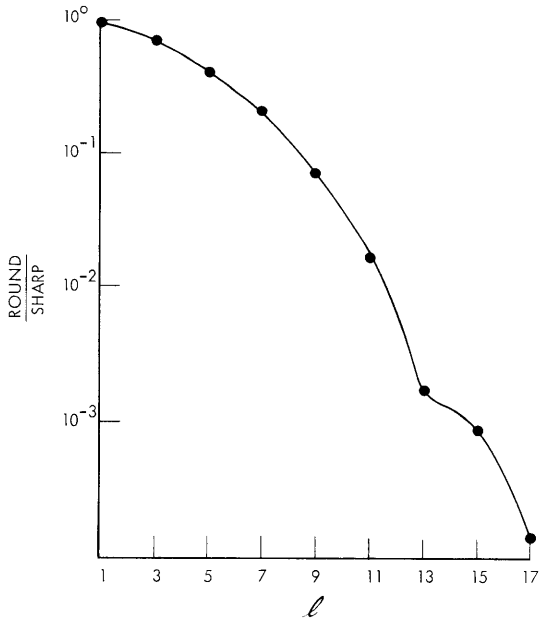

Fig. XVI-6. Ratio of calculated admittance for probe with a round edge to that of probe with a sharp edge.

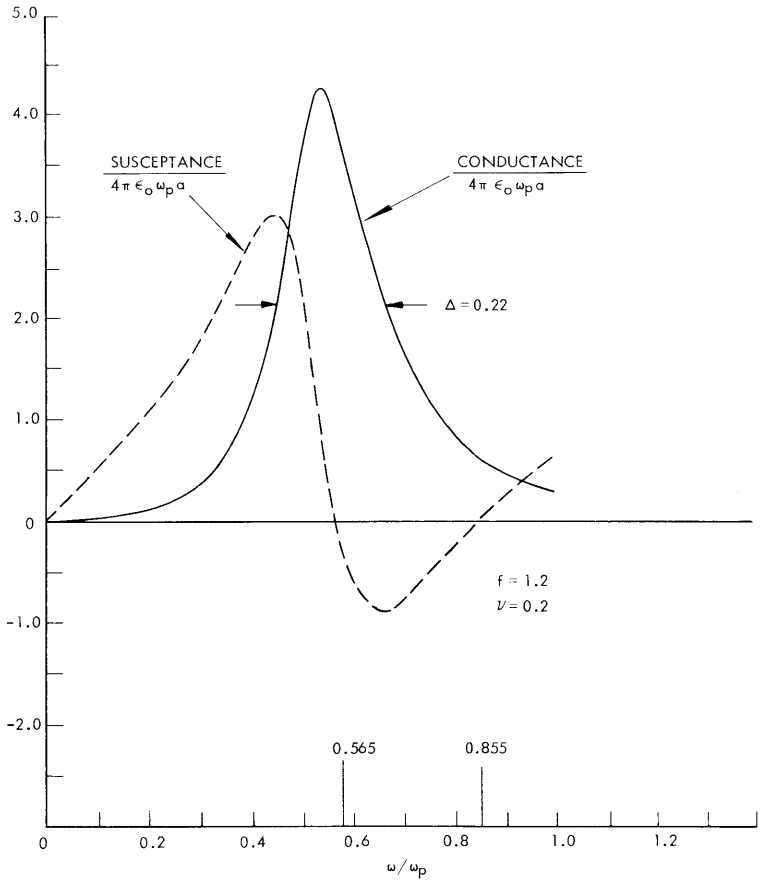

Fig. XVI-7. Theoretical admittance vs normalized frequency for probe with rounded edge.

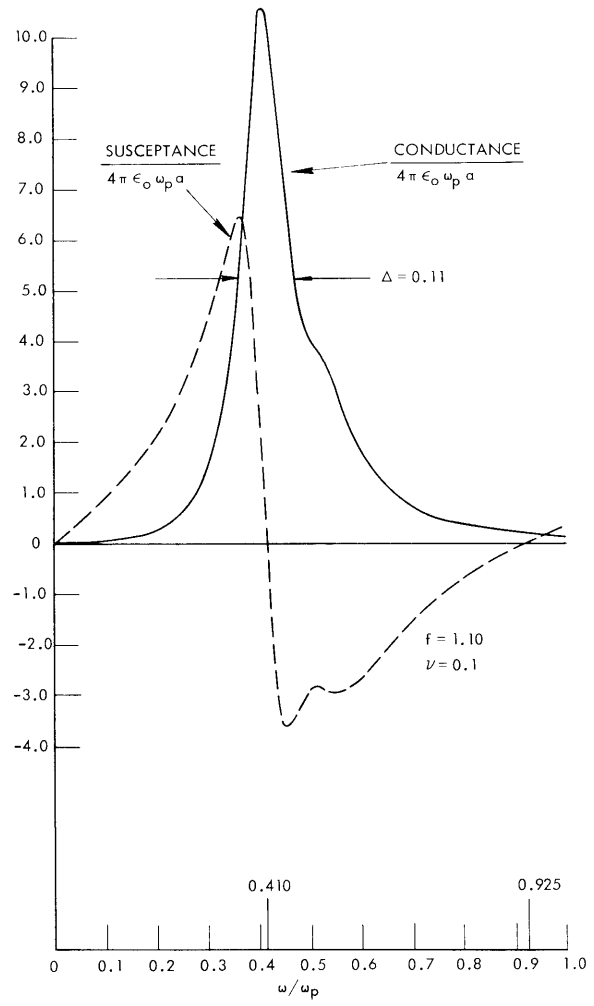

Fig. XVI-8. Theoretical admittance vs normalized frequency for probe with founded edge.

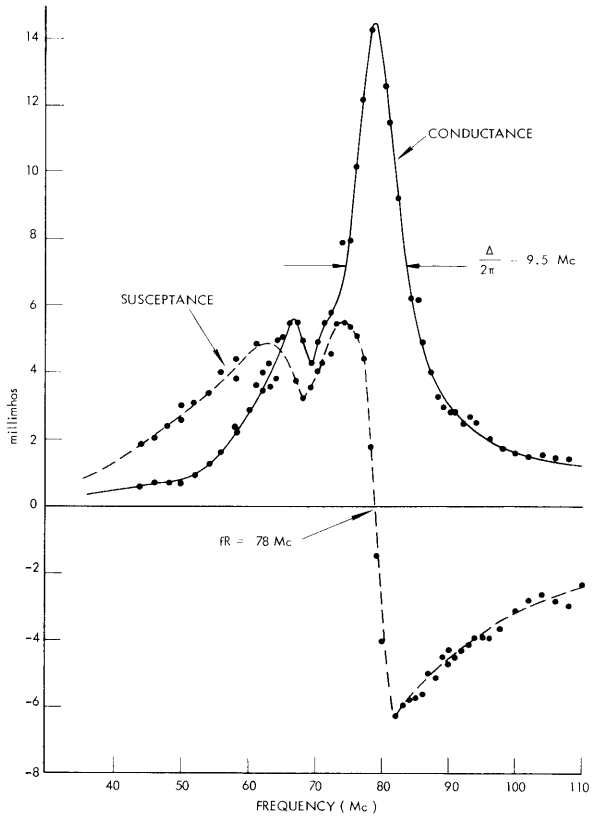

Fig. XVI-9. Measured admittance for a probe with 1.75-in. diameter.

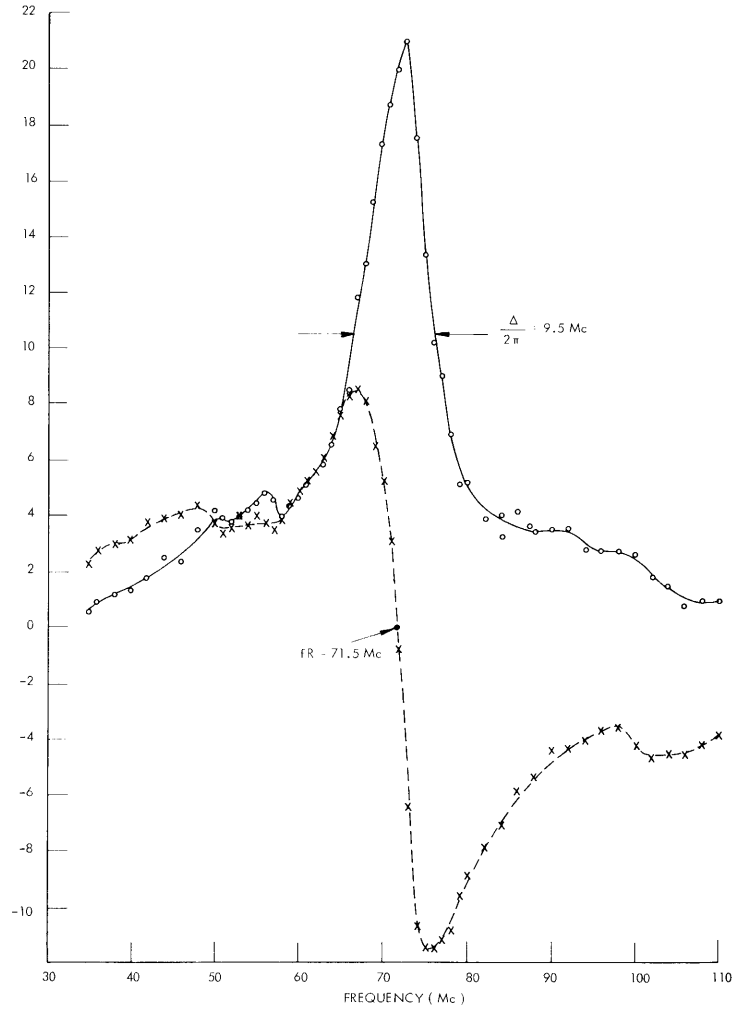

Fig. XVI-10. Measured admittance for a probe with 2-in. diameter.

the assumption that the presence of the plasma has a negligible effect on the potential in the region near the rounded corner (which is true if fringing fields do not penetrate the plasma), the potential, V, can be determined at r = R as a function of θ. We now have a spherical boundary condition, V = V(θ) at r = R, and the derivation proceeds as before.[1] Figure XVI-6 shows the effect of rounding the hemisphere edge on the solution for the admittance. Here, ℓ is the summation index in the series solution. Changing the gap size for the probe with the rounded edge has a negligible effect on its contribution to the admittance. Higher order terms are greatly reduced in magnitude and the series now converges rapidly.

Figures XVI-7 and XVI-8 are theoretical plots of the real and imaginary parts of the admittance of a round-edged probe. The admittance values are normalized to the free-space admittance of an ideal dipole at the plasma frequency. Here, f is the ratio of sheath radius (measured from center of probe) to the probe radius, and ν is the effective collision frequency normalized to the plasma frequency. In Fig. XVI-8 the contributions of terms in the series for $\ell > 1$ cause a kink in the admittance curves. An increase in ν causes the kink to disappear.

The experimental arrangement has been illustrated previously.[2] Figures XVI-9 and XVI-10 are representative plots of experimentally determined admittance curves. Data for Fig. XVI-9 was taken with a probe of 1.75-in. diameter, and for Fig. XVI-10 with a probe of 2-in. diameter. The plasma parameters for both cases are $n_o \approx 2.4\times10^{8}/cm^{3}$, $T_- \approx 5.1$ ev, and pressure $\approx 6 \times 10^{-4}$ mm Hg. Argon was the gas that was used.

Figures XVI-11 and XVI-12 are plots of the ratio of resonant frequency to plasma frequency as a function of probe size for constant plasma parameters. For Fig. XVI-11,

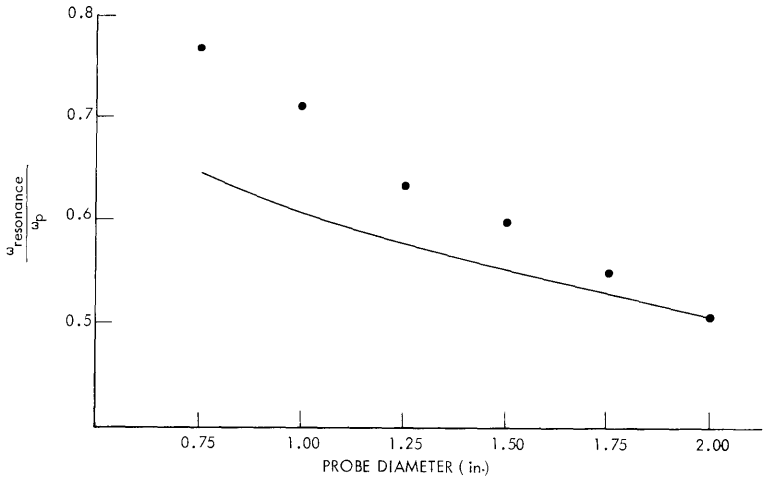

Fig. XVI-11. Ratio of resonant frequency to plasma frequency vs probe size.

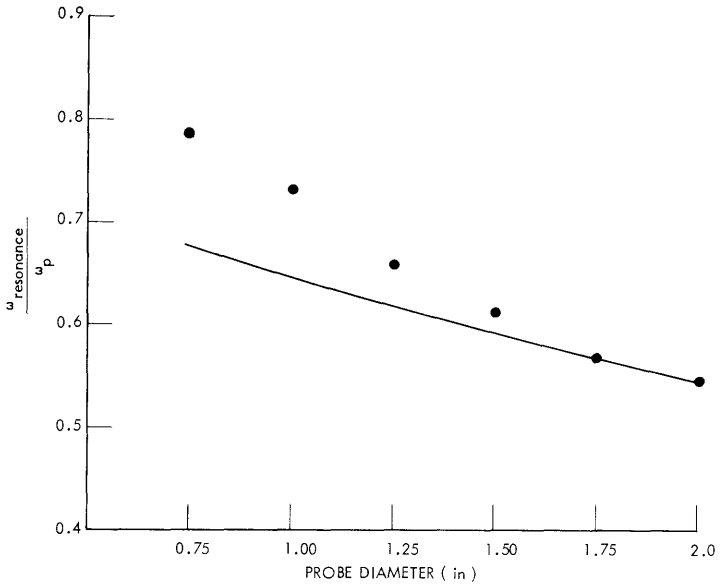

Fig. XVI-12. Ratio of resonant frequency to plasma frequency vs probe size.

$n_o \approx 2.4 \times 10^8/cm^3$, $T_- \approx 5.1$ ev, $p \approx 6 \times 10^{-4}$ mm Hg. For Fig. XVI-12, $n_o = 1.0 \times 10^8/cm^3$, $T_- \approx 3.0$ ev, $p = 6 \times 10^{-4}$ mm Hg. The curve drawn in each figure is the variation one gets, using the present theory, for the dipole term only when one assumes a constant sheath thickness. The curves have been fitted to the value for the 2.0-inch probe. The sheath thickness for the curve in Fig. XVI-11 is $4.6\ \lambda_D = 0.68$ in., and in Fig. XVI-12 it is $5.2\ \lambda_D = 0.51$ in.

The widths of the observed conductance peaks are wider than the theoretically predicted values ($\Delta \approx 1.1\ \nu$) by approximately a factor of 10. More data are being taken to determine experimentally the variation of peak widths on plasma parameters.

J. A. Waletzko

References

1. D. F. Smith and G. Bekefi, "Radiofrequency Probe," Quarterly Progress Report No. 74, Research Laboratory of Electronics, M. I. T., July 15, 1964, pp. 91-98.
2. J. A. Waletzko, "Radiofrequency Dipole Resonance Probe," Quarterly Progress Report No. 79, Research Laboratory of Electronics, M. I. T., October 15, 1965, pp. 95-98.